Mechanism for the Hydrolysis of Organophosphates by the Bacterial Phosphotriesterase†

Sarah D. Aubert,‡ Yingchun Li,§ and Frank M. Raushel*,‡,§

Department of Biochemistry and Biophysics, Texas A&M University, College Station, Texas 77843, and Department of Chemistry, P. O. Box 30012, Texas A&M University, College Station, Texas 77842-3012

Received January 30, 2004; Revised Manuscript Received March 16, 2004

ABSTRACT: Phosphotriesterase (PTE) from *Pseudomonas diminuta* is a zinc metalloenzyme that hydrolyzes a variety of organophosphorus compounds. The kinetic parameters of Zn/Zn PTE, Cd/Cd PTE, and a mixed-metal Zn/Cd hybrid PTE were obtained with a variety of substrates to determine the role of each metal ion in binding and catalysis. pH-rate profiles for the hydrolysis of diethyl *p*-nitrophenyl phosphate (**I**) and diethyl *p*-chlorophenyl phosphate (**II**) demonstrated that the ionization of a single group in the pH range of 5−10 was critical for substrate turnover. The pK_a values determined from the kinetic assays were dependent on the identity of the metal ion that occupied the α site within the binuclear metal center. These results suggest that the hydrolytic nucleophile is activated as a hydroxide via the ionization of a water molecule attached to the α-metal ion. The kinetic constants for the hydrolysis of **II** and diethyl *p*-chlorophenyl thiophosphate (**IV**) were determined for the metal substituted forms of PTE. The kinetic constants for **IV** were greater than those for **II**. The inverse thio effect is consistent with the polarization of the phosphoryl oxygen/sulfur bond via a direct ligation to the metal center. The rate enhancement is greater when Cd^{2+} occupies the β-metal-ion position. A series of alanine and asparagine mutations were used to characterize the catalytic roles of Asp233, His254, and Asp301. Mutations to either Asp233 or His254 resulted in an enhanced rate of hydrolysis for the sluggish substrate, diethyl *p*-chlorophenyl phosphate, and a decrease in the kinetic constants for paraoxon (**I**). These results are consistent with the existence of a proton relay from Asp301 to His254 to Asp233 that is used to ferry protons away from the active site with substrates that do not require activation of the leaving group phenol. A mechanism for the hydrolysis of organophosphates by the bacterial PTE has been proposed.

The enzyme phosphotriesterase (PTE)[1] was initially isolated from strains of soil bacteria that possessed the ability to hydrolyze organophosphate esters, including an array of agricultural pesticides and chemical warfare agents (*1*). The gene encoding PTE was found associated with a nonchromosomal plasmid and subsequently subcloned into a variety of expression vectors (*2*, *3*). PTE has no known natural substrates; however, the purified enzyme will hydrolyze insecticides such as paraoxon (**I**) with k_{cat} and k_{cat}/K_m values that approach 10^4 s^{-1} and 10^8 M^{-1} s^{-1}, respectively (*4*). Recently, PTE and other organophosphate degrading enzymes have become the focus of more intense scrutiny because of their demonstrated utility toward the detoxification of agricultural pesticides and chemical warfare agents (*5*−*7*). The enzymatic hydrolysis of **I** is presented in Scheme 1.

Scheme 1

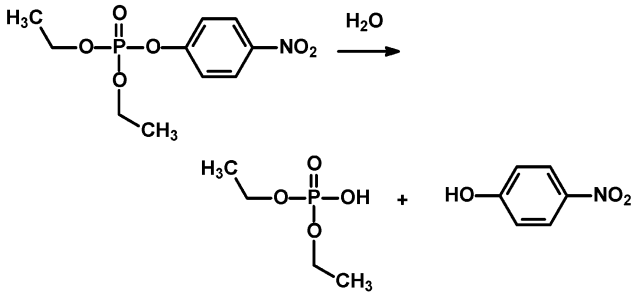

PTE from *Pseudomonas diminuta* has been extensively characterized using a variety of mechanistic, genetic, structural, and spectroscopic approaches. Experiments conducted in oxygen-18-labeled water with a chiral thiophosphonate substrate demonstrated that the cleavage of the P−O bond occurs via an S_N2-like single displacement reaction with a net inversion of the configuration at the phosphorus center (*8*). The enzyme has been crystallized and the three-dimensional X-ray structure shows that the protein folds as a $(\beta/\alpha)_8$ barrel (*9*). A binuclear metal center with two zinc ions is found at the active site of PTE. The five amino acids that are in direct coordination with the two metal ions are His55, His57, His201, His230, and Asp301. The metals are bridged by a carboxylated lysine (Lys169) and a molecule from the solvent. A representation of the binuclear metal

† This work was supported in part by the National Institutes of Health (GM 33894) and the Robert A. Welch Foundation (A-840).

* To whom correspondence should be addressed. Phone: 979-845-3373. Fax: 979-845-9452. E-mail: raushel@tamu.edu.

‡ Department of Biochemistry and Biophysics.

§ Department of Chemistry.

[1] Abbreviations: PTE, phosphotriesterase; DHO, dihydroorotase; HEPES, 4-(2-hydroxyethyl)-1-piperazineethanesulfonic acid; IPTG, isopropyl-D-thiogalactopyranoside; TABS, *N*-tris(hydroxymethyl)methyl-4-aminobutanesulfonic acid; MES, 2-morpholinoethanesulfonic acid; PIPES, piperazine-*N*,*N*′-bis(2-ethanesulfonic acid); TAPS, *N*-[tris(hydroxymethyl)methyl]-3-aminopropanesulfonic acid.

10.1021/bi0497805 CCC: $27.50
Published on Web 04/21/2004

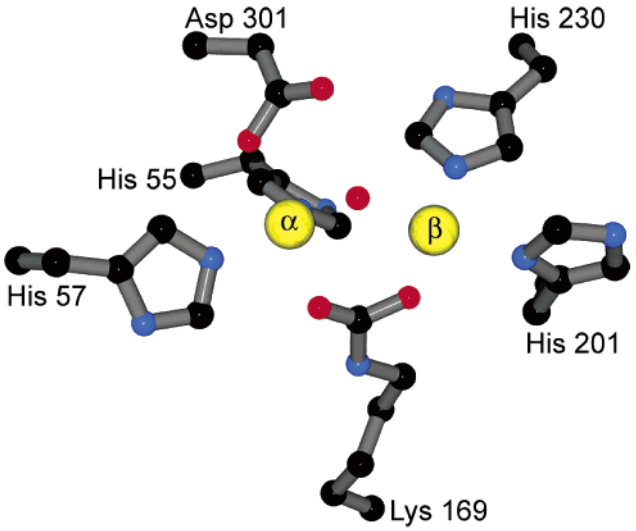

FIGURE 1: Structure of the binuclear metal center for the bacterial PTE. The coordinates are taken from Benning et al. (*22*) and can be obtained from the Protein Data Bank (PDB) (1HZY).

center in the active site of PTE is depicted in Figure 1. The two metal ions are designated as α and *β*. The α metal is more buried and is in direct coordination with His55, His57, and Asp301. The *β* metal is more solvent-exposed and is coordinated to His201 and His230. The native zinc ions at the active site can be replaced by reconstitution of the apoenzyme with Co^{2+}, Ni^{2+}, Cd^{2+}, or Mn^{2+} with retention of the catalytic activity (*4*). The general features of the protein fold and the specific ligand geometry of the binuclear metal center define the structural motif found in the amidohydrolase superfamily of enzymes (*10*). Other members of the amidohydrolase superfamily include, but are not limited to, urease, dihydroorotase, adenosine deaminase, and atrazine chlorohydrolase (*10*). Nearly all members of this superfamily utilize one or two divalent cations to activate a water molecule to initiate a nucleophilic attack on the substrate.

Despite the extensive amount of literature on PTE, some basic mechanistic questions remain to be answered. Previous investigations have shown that both metal ions are required for optimum catalytic activity; however, the specific role of each metal ion in the active site is unknown (*11*). Potential catalytic functions for one or both of the two metal ions include (*i*) polarization of the P═O or P═S bond of the substrate to increase the electrophilic character of the phosphorus center, (*ii*) activation of the hydrolytic water molecule, and (*iii*) neutralization of the developing negative charge on the leaving group during P−O bond cleavage. Moreover, the catalytic participation of other amino acid residues in substrate turnover has been largely unexplored. For example, the side-chain carboxylate of Asp301 is within hydrogen-bonding distance to the bridging hydroxide in the active site. A hydrogen-bonded network is apparently extended through direct interactions with His254 and Asp233. The orientation of these residues within the active site of PTE is shown in Figure 2. These two residues may function in concert with the binuclear metal center and Asp301 to shuttle protons from the active site to the bulk solvent during substrate turnover. In addition, the side chain of Tyr309 has been proposed from molecular-dynamic calculations as a stabilizing factor for the developing negative charge of the *p*-nitrophenolate leaving group of **I** (*12*).

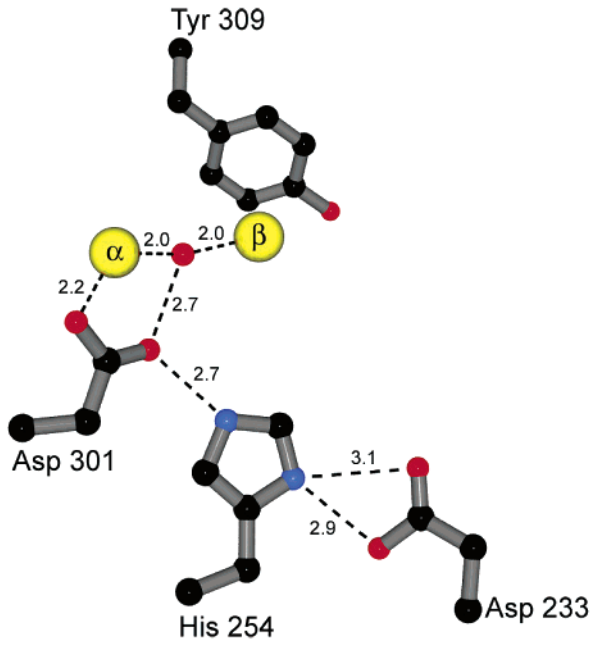

FIGURE 2: Orientation of the active-site residues examined in this paper. The coordinates were taken from Benning et al. (*22*) and can be obtained from the PDB (1HZY).

Chart 1

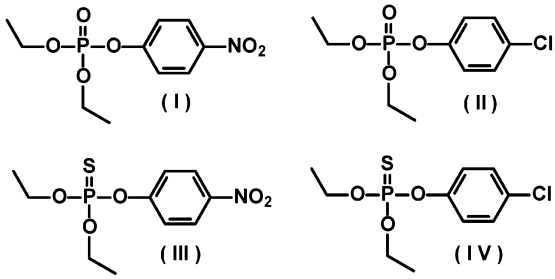

The enzymatic properties of PTE make this protein an ideal candidate for mechanistic interrogation. In this paper, the relative functions of the twin zinc ions found in the active site are addressed through characterization of the catalytic properties of PTE substituted with other transition-metal ions. The differential roles played by each of the two divalent cations are probed via the construction of a hybrid binuclear metal center with zinc and cadmium at unique sites in the same active site. The enhancement of the electrophilic character of the phosphorus center is ascertained through the utilization of phosphate and thiophosphate triesters as the substrates. Phosphorus−oxygen bond cleavage events and proton transfers are disentangled from one another through the use of substrates with altered rate-limiting steps. The specific roles of individual amino acid side chains are determined by the construction and characterization of site-directed mutants.

MATERIALS AND METHODS

Materials. **I** was purchased from Sigma and further purified to remove *p*-nitrophenol (*4*). Diethyl *p*-chlorophenyl phosphate (**II**), parathion (**III**), and diethyl *p*-chlorophenyl thiophosphate (**IV**) were synthesized as previously described (*13*, *14*). The structures of these substrates are presented in Chart 1. All other chemicals used in this paper were purchased from Aldrich, Sigma, Fisher Scientific, or United

States Biochemical Co. Wizard miniprep DNA purification kit was purchased from Promega. Deuterium oxide (99.9%) and methanol-d_4 (99.8%) were purchased from Cambridge Isotope Laboratories. Oligonucleotide synthesis and DNA sequencing reactions were performed by the Gene Technology Laboratory of Texas A&M University.

Construction of PTE Mutants. Site-directed mutagenesis was performed using the template plasmid pJK01 or pJW01. The mutants D301A, D301N, and H254N were constructed using the overlap extension method of PCR (*15*) by Kuo et al. (*16*). The mutants H254A, D233A, D233N, and Y309F were made with the QuikChange site-directed mutagenesis kit from Stratagene. The mutated plasmids were sequenced to ensure the fidelity of the PCR reactions.

Purification of PTE. Plasmids harboring the wild-type and mutant PTE genes were transformed into *E. coli* BL-21 cells. A single colony was used to inoculate a 6-mL overnight culture of LB broth containing 50 μg/mL ampicillin. The overnight culture was used to inoculate 1.0 L of TB media containing 1.0 mM $CoCl_2$ and 50 μg/mL ampicillin (*3*). The cobalt-supplemented growth medium was incubated in a shaker at 30 °C. After incubation for 20 h, 400 μM isopropyl-D-thiogalactopyranoside (IPTG) was added. The cells were harvested by centrifugation 36 h after induction. PTE was purified according to the published procedures (*4*). The cells were lysed by sonication with 5-s pulses for 40 min at 4 °C. After centrifugation, the nucleic acids were removed by adding 2% (w/v) protamine sulfate dropwise. After centrifugation, ammonium sulfate was added to a saturation of 45%. The pellet from the ammonium sulfate step was resuspended in the purification buffer and loaded onto a 5.0 × 150 cm gel filtration column containing Ultrogel AcA 54 (IBF) and eluted at a flow rate of 1.0 mL/min. The fractions were pooled based on the catalytic activity. DEAE-Sephadex A-25 (Sigma) was equilibrated in the purification buffer (pH 8.5) and incubated with the protein pooled from the gel filtration step at 4 °C overnight. The PTE was eluted from the column by washing with 4 column volumes of a pH 8.5 purification buffer. The purity of the protein was verified by sodium dodecyl sulfate-polyacrylamide gel electrophoresis.

Preparation and Reconstitution of apo-PTE. Wild-type and mutant enzymes were rendered metal-free by incubation with 2.0 mM 1,10-phenanthroline at 4 °C until less than 1% of the original catalytic activity remained. The chelator was removed by diafiltration using an Amicon diafiltration device and a 50 mM HEPES buffer (pH 8.0) until less than 1.0 nM 1,10-phenanthroline remained (*4*). The 50 mM HEPES buffer (pH 8.0) was passed through a Chelex-100 column to remove excess metal. All glassware used for metal-ion reconstitution was washed with 30% nitric acid and rinsed with deionized water. The apo-PTE was reconstituted with 2 equiv of $ZnCl_2$ and $CdCl_2$, or 1 equiv of $ZnCl_2$ and $CdCl_2$. The metal content of the metal-substituted PTE was verified using a Perkin−Elmer AAnalyst 700 atomic absorption spectrometer with an acetylene-air flame.

Kinetic Measurements and Data Analysis. Throughout the purification of PTE, the catalytic activity of metal-substituted wild-type or mutant PTE was assayed by measuring the release of *p*-nitrophenol ($\epsilon = 17.0$ mM^{-1} cm^{-1}) spectrophotometrically at 400 nm in a 30 mM TABS buffer (pH 9.0) with 1.0 mM **I**. Reaction rates were determined with a Gilford model 260 spectrophotometer at 25 °C. No extra metal was added to the assay mixture but all enzyme dilutions were performed with a 50 mM HEPES buffer (pH 8.0) and 100 μM desired metal. The Zn/Cd metal hybrid was not diluted into a metal-containing buffer.

The kinetic parameters, k_{cat} and k_{cat}/K_m, were determined spectrophotometrically using a SPECTRAmax-340 microplate spectrophotometer at 30 °C (Molecular Devices Inc.). The enzyme-catalyzed hydrolysis of **I** (50−3000 μM), **II** (50−3000 μM), **III** (20−250 μM), and **IV** (20−250 μM) was performed in a 30 mM TABS buffer (pH 9.0) and 20% methanol, because of the limited solubility of the thiophosphate substrates. The reaction was followed spectrophotometrically by measuring the formation of either *p*-nitrophenol at 347 nm ($\epsilon = 5176$ M^{-1} cm^{-1}) or *p*-chlorophenol at 283 nm ($\epsilon = 1243$ M^{-1} cm^{-1}). These are the isosbestic wavelengths for the substituted phenol and corresponding phenolate, and thus the reaction can be monitored at a single wavelength that is independent of pH. The values of k_{cat} and k_{cat}/K_m were determined by fitting the initial velocity data to eq 1, where v is the initial velocity, k_{cat} is the turnover number, E_t is the enzyme concentration, A is the substrate concentration, and K_m is the Michaelis constant.

$$v/E_t = k_{cat}A/(K_m + A) \quad (1)$$

The pH-rate profiles were determined for the Zn/Zn, Cd/Cd, and Zn/Cd forms of the wild-type PTE with **I** and **II** as the substrates. Each metal variant of PTE was assayed over a pH range of 5.0−10.0 at 0.2 pH unit increments. The buffers MES (5.1−6.5), PIPES (6.6−7.2), HEPES (7.3−8.2), TAPS (8.3−8.9), and TABS (9.0−10.1) were used separately at a concentration of 30 mM. The final pH was measured at the end of the enzymatic reaction. The pK_a values from the pH-rate profiles were determined by fitting the data to eq 2 or 3, where y is k_{cat} or k_{cat}/K_m, c is the pH independent value of y, H is the hydrogen-ion concentration, and K_a is the dissociation constant of the ionizable group.

$$\log y = \log [c/(1 + H/K_a)] \quad (2)$$

$$\log y = \log [c/(1 + H^2/K_a^{\,2})] \quad (3)$$

The kinetic constants, k_{cat} and k_{cat}/K_m were determined for **I** and **II** in water or 99% D_2O with the metal-substituted wild type and selected zinc-substituted mutants of PTE. The solvent deuterium isotope effects were determined over a pH range of 8.6−10.0. Stock solutions of a 0.5 M TAPS buffer (8.6−8.9) and TABS buffer (9.0−10.0) were made with 99% D_2O, and the pH was adjusted with 10 M KOH. Because of the limited solubility of **II**, 99% methanol-d_4 was added to a final methanol concentration of 20%. For the activity assays, all PTE dilutions were made with a 99% D_2O HEPES buffer (50 mM, pH 8.5). The pH values were determined at the end of the reaction by adding 0.4 to the pH-electrode reading (*17*).

RESULTS

Kinetic Properties of Metal-Substituted PTE. The values of K_m, k_{cat}, and k_{cat}/K_m for the hydrolysis of the organophosphate triesters **I**−**IV** at pH 9.0 are listed in Table 1 for the Zn/Zn, Cd/Cd, and Zn/Cd metal-substituted forms of the

Table 1: Kinetic Parameters for the Hydrolysis of Phosphotriesters by Metal-Substituted Variants of Wild-Type PTE[a]

	Zn/Zn			Cd/Cd			Zn/Cd		
substrate	K_m (mM)	k_{cat} (s^{-1})	k_{cat}/K_m (M^{-1} s^{-1})	K_m (mM)	k_{cat} (s^{-1})	k_{cat}/K_m (M^{-1} s^{-1})	K_m (mM)	k_{cat} (s^{-1})	k_{cat}/K_m (M^{-1} s^{-1})
I	0.34 ± 0.03	2300 ± 60	$6.8(0.5) \times 10^6$	1.9 ± 0.2	2500 ± 200	$1.32(0.09) \times 10^6$	0.74 ± 0.07	2060 ± 80	$2.8(0.2) \times 10^6$
II	1.6 ± 0.3	0.36 ± 0.03	220 ± 20	7.0 ± 0.5	0.23 ± 0.05	33 ± 2	3.3 ± 0.8	0.13 ± 0.02	39 ± 3
III	1.5 ± 0.4	720 ± 190	$4.8(0.2) \times 10^5$	1.7 ± 0.6	600 ± 200	$3.5(0.1) \times 10^5$	0.6 ± 0.1	300 ± 40	$5.0(0.2) \times 10^5$
IV	0.5 ± 0.2	2.2 ± 0.6	4400 ± 400	0.3 ± 0.1	1.1 ± 0.2	4000 ± 500	0.6 ± 0.2	2.4 ± 0.5	4100 ± 280

[a] All kinetic parameters were determined at pH 9.0 in 20% methanol. The kinetic constants were obtained by a fit of the data to eq 1.

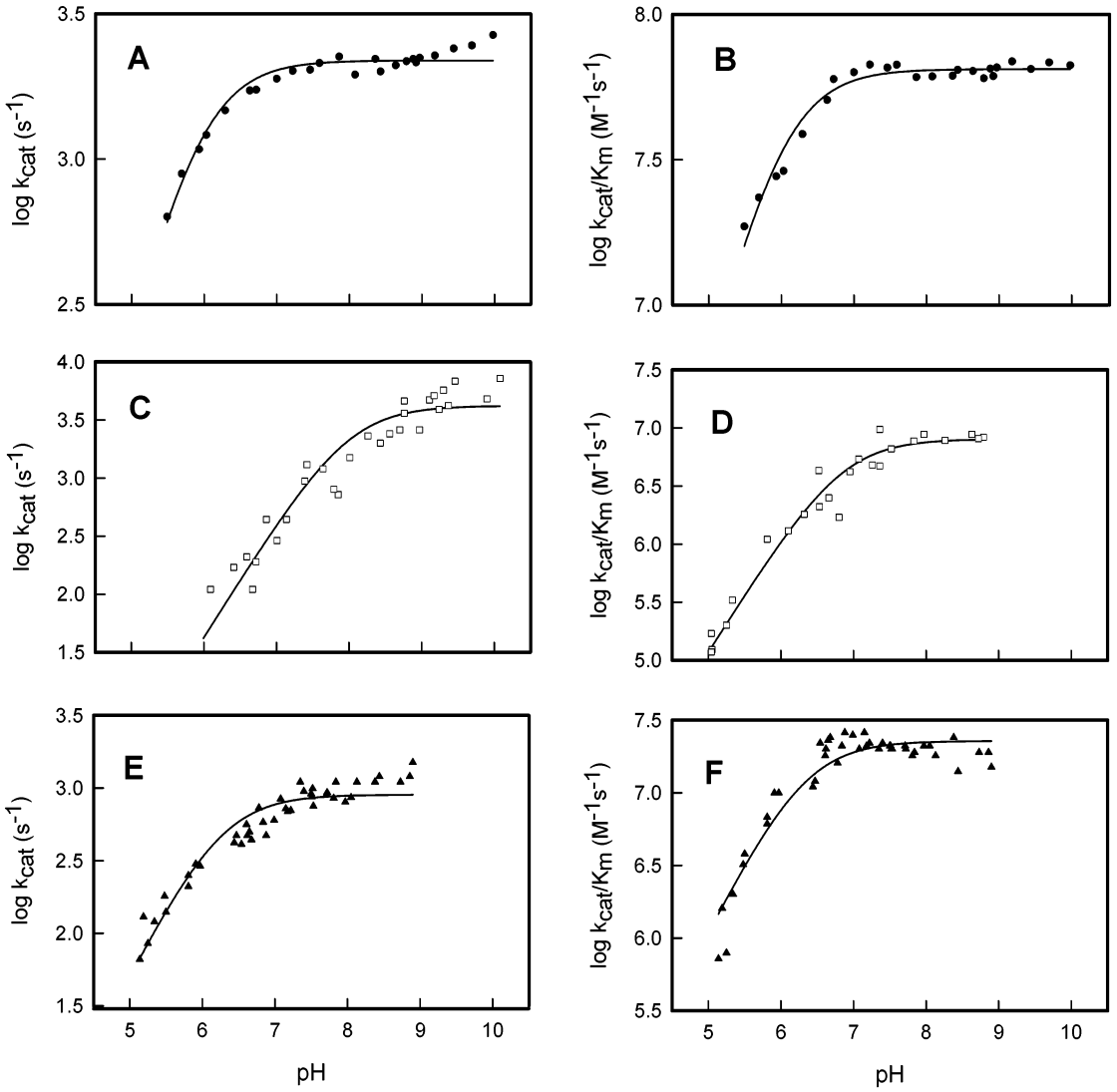

FIGURE 3: pH-rate profiles for the hydrolysis of **I** with Zn/Zn PTE (●), Cd/Cd PTE (□), and Zn/Cd PTE (▲). The data were fit to eq 2. Additional details are provided in the text.

wild-type PTE. The metal-substituted enzymes hydrolyze the substrates **I** and **III** anywhere from 100 to 10 000 times faster than the substrates **II** and **IV**.

pH-Rate Profiles of Metal-Substituted PTE. The pH dependence of the kinetic parameters, k_{cat} and k_{cat}/K_m, was determined with **I** and **II** as the substrates. The log k_{cat} versus pH-rate profiles for the enzymatic hydrolysis of **I** are presented in Figure 3 for the Zn/Zn, Cd/Cd, and Zn/Cd substituted forms of PTE. The pH-rate profiles in Figure 3 indicate that a single group must be deprotonated for optimum activity. The metal-substituted PTE variants show that the specific metal ion within the active site modulates the pK_a values determined from the kinetic assays for both **I** and **II** hydrolysis. For **I** hydrolysis, Zn/Zn PTE has a pK_a value for k_{cat} of 5.9, which is similar to the pK_a of 6.2 obtained for Zn/Cd PTE. In contrast, Cd/Cd PTE has a higher pK_a value of 8.0. The pK_a values for k_{cat}/K_m of **I** hydrolysis are 6.0, 6.3, and 6.9 for Zn/Zn, Zn/Cd, and Cd/Cd PTE, respectively. A similar trend is observed for the pK_a values determined with the slow substrate, **II**. The kinetic pK_a values from the pH-rate profiles for k_{cat} are 5.7, 6.0, and 7.4 for Zn/Zn, Zn/Cd, and Cd/Cd PTE hydrolysis of **II**. For k_{cat}/K_m, Zn/Zn, Zn/Cd, and Cd/Cd PTE have pK_a values from the pH-rate profiles of 6.2, 5.9, and 6.4, respectively. The pK_a values, from fits of the data to eq 2, are presented in Table 2.

Table 2: pK_a Values for Metal-Substituted PTE from pH-Rate Profiles in H_2O and D_2O[a]

		Zn/Zn		Cd/Cd		Zn/Cd	
substrate	solvent	k_{cat} (s^{-1})	k_{cat}/K_m (M^{-1} s^{-1})	k_{cat} (s^{-1})	k_{cat}/K_m (M^{-1} s^{-1})	k_{cat} (s^{-1})	k_{cat}/K_m (M^{-1} s^{-1})
I	H_2O	5.9 ± 0.1	6.0 ± 0.1	8.0 ± 0.1	6.9 ± 0.1	6.2 ± 0.1	6.3 ± 0.1
II[b]	H_2O	5.7 ± 0.1	6.2 ± 0.1	7.4 ± 0.1	6.4 ± 0.1	6.0 ± 0.1	5.9 ± 0.1
I	D_2O	6.5 ± 0.1	6.3 ± 0.1	8.5 ± 0.1	7.4 ± 0.1	7.0 + 0.1	6.8 + 0.1
II[b]	D_2O	6.1 ± 0.1	6.0 ± 0.1	7.9 ± 0.1	6.6 ± 0.1	6.4 + 0.1	6.5 + 0.1

[a] Values from a fit of the data to eq 2 over a pH range of 5.0−10.0. [b] Values determined in 10% methanol-d_4.

Table 3: Solvent Deuterium Isotope Effects with Metal-Substituted PTE[a]

	Zn/Zn		Cd/Cd		Zn/Cd	
substrate	$^{D_2O}k_{cat}$ (s^{-1})	$^{D_2O}k_{cat}/K_m$ (M^{-1} s^{-1})	$^{D_2O}k_{cat}$ (s^{-1})	$^{D_2O}k_{cat}/K_m$ (M^{-1} s^{-1})	$^{D_2O}k_{cat}$ (s^{-1})	$^{D_2O}k_{cat}/K_m$ (M^{-1} s^{-1})
I	2.0 ± 0.2	1.05 ± 0.06	2.6 ± 0.4	0.9 ± 0.1	1.8 ± 0.2	1.0 ± 0.1
II[b]	1.3 ± 0.1	0.95 ± 0.07	1.5 ± 0.3	1.0 ± 0.2	1.4 ± 0.1	0.92 ± 0.08

[a] Kinetic parameters determined over a pH range of 8.6−10.0. [b] Values determined in 10% methanol-d_4.

Table 4: Kinetic Parameters of Wild-Type and Mutant Zn/Zn PTE with Substrates **I** and **II**[a]

substrate	**I**			**II**		
enzyme	k_{cat} (s^{-1})	k_{cat}/K_m (M^{-1} s^{-1})	K_m (mM)	k_{cat} (s^{-1})	k_{cat}/K_m (M^{-1} s^{-1})	K_m (mM)
wild type	2300 ± 60	6.8(0.5) × 10^6	0.34 ± 0.03	0.36 ± 0.03	220 ± 20	1.6 ± 0.26
D233A	280 ± 10	4.9(0.4) × 10^5	0.57 ± 0.07	4.4 ± 0.2	1310 ± 40	3.4 ± 0.3
D233N	680 ± 20	7.8(0.4) × 10^5	0.87 ± 0.06	0.88 ± 0.09	400 ± 40	2.2 ± 0.4
H254A	220 ± 10	1.6(0.1) × 10^6	0.14 ± 0.02	12 ± 4	1400 ± 100	9.0 ± 3.0
H254N	17.8 ± 0.3	8.6(0.8) × 10^5	0.021 ± 0.002	0.56 ± 0.02	640 ± 30	0.87 ± 0.09
D301A	11.2 ± 0.5	3.3(0.3) × 10^4	0.34 ± 0.04	0.015 ± 0.001	60 ± 10	0.26 ± 0.08
D301N	0.55 ± 0.02	2.8(0.2) × 10^3	0.20 ± 0.02	<0.006		
Y309F	1700 ± 260	2.3(0.5) × 10^6	0.8 ± 0.2	0.24 ± 0.04	79 ± 8	3.0 ± 0.8

[a] All kinetic parameters were determined at pH 9.0 in 20% methanol.

Solvent Deuterium Isotope Effects. The pH-rate profiles for both **I** and **II** hydrolysis by metal-substituted variants of PTE were determined in 99% D_2O (Table 2). The pK_a values determined in D_2O range from 0.2 to 0.8 pK_a units higher than the pK_a values determined in water. The pK_a values, from the kinetic assays in D_2O, follow a trend similar to the corresponding values obtained in water for the metal-substituted variants of PTE. The solvent deuterium isotope effects were determined over the pH-independent range of the pH-rate profiles (8.6−10.0) with **I** and **II** as the substrates. Shown in Table 3 are the solvent deuterium isotope effects for substrates **I** and **II** with Zn/Zn, Cd/Cd, and Zn/Cd PTE. With **I**, the solvent isotope effects the range from 1.8 to 2.6 for k_{cat} and are essentially in unity with k_{cat}/K_m. With the slower substrate **II**, the solvent isotope effects on k_{cat} are small (1.3−1.5) and in unity with k_{cat}/K_m.

Kinetic Properties of Zn/Zn-Substituted PTE Mutants. The kinetic parameters of Zn/Zn-substituted mutants at amino residues D233, H254, D301, and Y309 of PTE were determined with substrates **I** and **II**, and the results are presented in Table 4. The X-ray crystal structure of PTE suggests that Asp233, His254, and Asp301 form a hydrogen-bonded link to the hydroxide that bridges the two divalent cations in the active site. In addition, molecular-dynamic simulations suggest that Tyr309 may play a role in the stabilization of the leaving group via an interaction with the nitro substituent of **I** (*12*). However, with the mutant Y309F, there is no significant difference in the magnitude of either k_{cat} or k_{cat}/K_m when compared to the wild-type enzyme for the hydrolysis of either **I** or **II**. Therefore, this residue does not appear to be significant in the determination of the catalytic properties of PTE.

Asp301 is a primary ligand to the α-metal ion in the binuclear metal center and is apparently hydrogen-bonded to the hydroxide that bridges the two metal ions. When this residue is mutated to either alanine or asparagine, there is a substantial drop in the catalytic activity of 2−3 orders of magnitude relative to the wild-type enzyme using either **I** or **II** as the substrate. The shape of the pH-rate profile for D301A is similar to that of the wild-type enzyme. The pK_a values, from fits of the data to eq 2, are 5.7 ± 0.1 and 6.0 ± 0.1 for k_{cat} and k_{cat}/K_m, respectively. With the mutant D301N, the pK_a values for the change in pH on the kinetic parameters, k_{cat} and k_{cat}/K_m, are 5.8 ± 0.1 and 5.9 ± 0.1, respectively. The solvent deuterium isotope effects on k_{cat} for **I** hydrolysis are 1.9 ± 0.1 and 1.4 ± 0.1 for D301A and D301N, respectively. For either mutant, the solvent deuterium isotope effects on k_{cat}/K_m are in unity.

The ϵ2 nitrogen from the imidazole size chain of His254 is 2.7 Å away from the nearest oxygen from the carboxylate side chain of Asp301. When His254 is mutated to either alanine or asparagine, there is a 1−2 order of magnitude reduction in the kinetic parameters when **I** is used as the substrate, but remarkably, there is a 2−33-fold *increase* in the kinetic parameters for the slow substrate **II** (Table 4). The pH-rate profile for the mutant H254A is similar in shape to that of the wild-type enzyme, except that the diminution in the log k_{cat}/K_m profile at a low pH occurs with a slope of ~2, indicating the ionization of the two groups with nearly identical pK_a values. A fit of the data to eq 3 is shown in

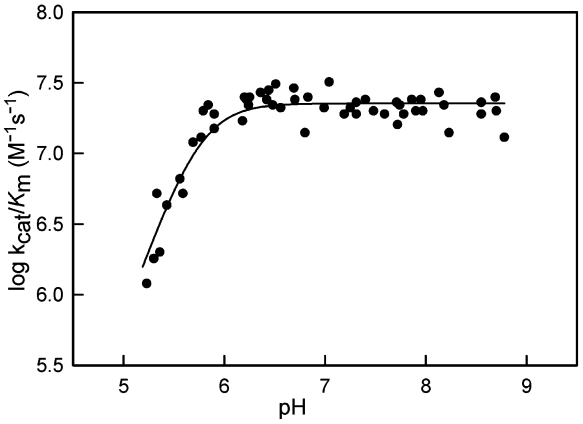

FIGURE 4: pH-rate profile of Zn/Zn-substituted H254A for the hydrolysis of **I**. The data were fit to eq 3. Additional details are provided in the text.

Scheme 2

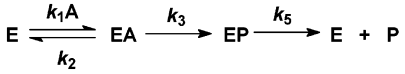

Figure 4 with a pK_a of 5.8. The pH-rate profile for k_{cat} was fit to eq 2 with a pK_a of 5.8. The solvent deuterium isotope effects were determined for the hydrolysis of **I** with H254A and H254N. In the pH-independent range of the pH-rate profile, the solvent deuterium isotope effects are 2.5 ± 0.1 and 2.1 ± 0.1 on k_{cat} for H254A and H254N, respectively. There is no measurable effect (1.0 ± 0.1) on k_{cat}/K_m for either mutant enzyme.

The two oxygens from the side-chain carboxylate of D233 are 2.9 and 3.1 Å away from the δ1 nitrogen of the side chain from His254. Asp233 was mutated to alanine and asparagine. With either of these mutations, there is a ~10-fold reduction in k_{cat} and k_{cat}/K_m for **I** hydrolysis. However, with D233N, there is a 2−3-fold *increase* in k_{cat} and k_{cat}/K_m for the slow substrate **II**. The net increase in the magnitude of the kinetic parameters is even more pronounced with D233A, where k_{cat} and k_{cat}/K_m increase by factors of 12 and 6, respectively, relative to the wild-type enzyme. The solvent deuterium isotope effects for the hydrolysis of **I** are 2.1 ± 0.1 and 1.9 ± 0.1 for D233A and D233N, respectively. There is no effect on k_{cat}/K_m by solvent deuterium for either mutant enzyme.

DISCUSSION

Kinetic Model. A minimal kinetic model for the hydrolysis of organophosphate esters by the bacterial PTE is presented in Scheme 2. In this scheme, there is a reversible binding step for the formation of the Michaelis complex (EA). This is followed by an irreversible cleavage of the P−O bond to generate an enzyme product complex (EP). In the final step, the products are released and the free enzyme (E) is regenerated. The last step in this simplified mechanism is actually a composite for the release of the two products and activation of the hydrolytic solvent.

In this scheme, the relationships for k_{cat} and k_{cat}/K_m are given in eqs 4 and 5, respectively. It has been shown previously that the rate-limiting step for either k_{cat} or k_{cat}/K_m can be cleanly titrated by changing the pK_a of the leaving-group phenol (*14*). With slow substrates, such as **II**, the rate-limiting step for either k_{cat} or k_{cat}/K_m is the cleavage of the P−O bond (k_3), whereas for the fast substrates, like **I**, the chemical step is fast, and thus, k_{cat} is primarily limited by k_5 and k_{cat}/K_m by k_1. We have used these two substrates to act as reporters for the different steps in the reaction mechanism. The Brønsted plot for a series of leaving-group phenols is nonlinear, reflecting the distinct change in rate-limiting steps (*14*). The β value from the Brønsted plot in the regime, where P−O bond cleavage is rate-liming, is −2.2 for Zn/Zn PTE (*18*). This indicates that the bond cleavage in the transition state is well-advanced.

$$k_{cat} = (k_3k_5)/(k_3 + k_5) \quad (4)$$

$$k_{cat}/K_m = (k_1k_3)/(k_2 + k_3) \quad (5)$$

Activation of Water. The most logical candidate for the nucleophile that attacks the phosphoryl center is the solvent molecule that bridges the two divalent cations in the active site of PTE. Catalytic activity is lost for wild-type PTE at a low pH because of the protonation of a single group. Because the substrate does not ionize in the pH range of 5−10, the critical ionization must originate with the enzyme. The pK_a from the pH-rate profiles changes with the identity of the divalent cation bound to the active site. With Zn/Zn PTE, the value is 5.7 for the effect on k_{cat} with substrate **II** and increases to 7.4 for Cd/Cd PTE. Similar changes are observed on k_{cat}/K_m and with the faster substrate, **I**. This trend is consistent with the ionization of a metal-bound water molecule that gives rise to the active form of the enzyme. In aqueous systems, the pK_a of water bound to Zn^{2+} is 8.9, whereas it is 10.1 when bound to Cd^{2+} (*19*). In addition, a biomimetic chemical analogue of a binuclear Zn^{2+} complex has been reported to have a pK_a for the bridging hydroxide of 6.8 (*20*). Nevertheless, the utility of a bridging hydroxide as the specific nucleophile in binuclear enzyme centers has been questioned (*21*). However, all X-ray structures of PTE determined to date have a bridging water/hydroxide bound between the two divalent cations (*22*). In the uncomplexed form of Zn/Zn PTE, there is one additional water molecule bound to M_β. However, this water molecule is displaced upon binding of the substrate analogues, and thus, the only species available for nucleophilic attack is the bridging hydroxide (*23*, *24*). It is therefore proposed that the active site nucleophile is in the form of a hydroxide that bridges the two divalent cations in the active site of PTE. This conclusion is also supported by the pH variation of the antiferromagnetic coupling observed in Mn/Mn PTE.[2]

The dominance of the two divalent cations within the active site of PTE was addressed through the use of a mixed-metal hybrid enzyme. It has previously been shown that a unique Zn/Cd PTE could be prepared. ^{113}Cd NMR experiments demonstrated that a single mixed-metal hybrid was formed (*25*). High-resolution X-ray crystallography of the Zn/Cd hybrid enzyme showed that Zn^{2+} was bound to the more buried or α site, while the Cd^{2+} was bound to the more solvent exposed or β site (*22*). In the experiments conducted in this investigation, the pH-rate profiles for the Zn/Cd

[2] Cynthia Samples and Professor Victoria DeRose (Texas A&M University).

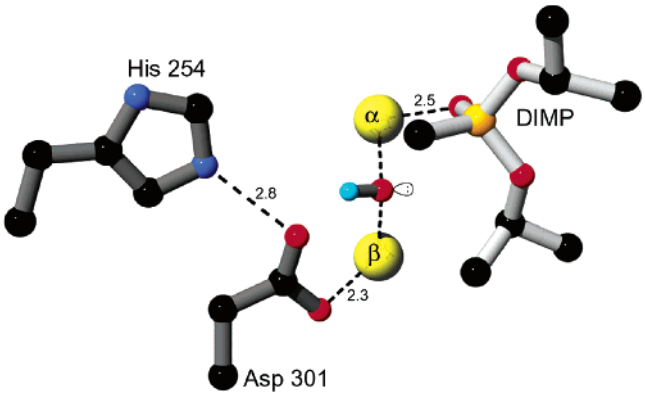

FIGURE 5: Relative orientation of the hydroxide bound to the binuclear metal center and the inhibitor DIMP in the bacterial PTE (PDB 1EZ2). The proposed orientation of the hydrogen and lone pair on the bridging hydroxide are shown for discussion purposes only.

enzyme more closely resembled Zn/Zn PTE than Cd/Cd PTE. Therefore, the identity of the metal ion that occupies the α site dominates the pK_a value for the bridging hydroxide ion.

Activation of the Substrate. The binuclear metal center can be utilized to activate the substrate for nucleophilic attack by polarization of the phosphoryl−oxygen bond. For the pair of substrates that are limited by P−O bond cleavage (**II** and **IV**), there is an enhancement in the value of k_{cat} and k_{cat}/K_m for hydrolysis of thiophosphate triester (**IV**) relative to phosphate ester hydrolysis (**II**). The ratio of the rate constants ranges from 5 to 120 in favor of the thiophosphate triester for the three-metal-substituted forms of PTE. This trend is opposite to what is observed if these same esters are hydrolyzed chemically by KOH (*18*). The inverse thio effect is consistent with the direct interaction of the phosphoryl oxygen and sulfur with one or more of the metals in the binuclear metal center. The dominance of the α- or *β*-metal ion for this effect is more difficult to assign. However, it should be noted that the enhancement in k_{cat}/K_m for the hydrolysis of the thiophosphate triester **IV** over the slower phosphate triester **II** with the Cd/Cd PTE and Zn/Cd PTE is 120 and 105, respectively, whereas the relative enhancement for Zn/Zn PTE is only 20. The primary role of the *β*-metal ion for the polarization of the phosphoryl−oxygen/sulfur bond is also supported by the X-ray structure of the substrate analogue, diisopropyl methyl phosphonate. The phosphoryl oxygen of the bound inhibitor is within 2.5 Å of the *β* metal and 4.4 Å of the α metal (*23*). In addition, the primary role of the *β*-metal ion toward the activation of the electrophile is supported by the X-ray crystal structure of dihydroorotase liganded by the substrate and product in the same crystal (*26*).

Activation of the Leaving Group. The substantial *β* value obtained previously from the Brønsted plots indicates that the transition state for phosphotriester hydrolysis is very late and that there is apparently no activation of the leaving group by the enzyme. The previous suggestion that the developing charge on the leaving groups such as *p*-nitrophenol could be neutralized via a partial proton transfer from the phenolic hydroxyl of Tyr309 was tested by mutation of this residue to phenylalanine. However, there was no measurable difference in the kinetic constants for any of the substrates tested in comparison between the wild-type enzyme and Y309F. Therefore, this residue does not contribute to the catalytic enhancement for the hydrolysis of organophosphates by the bacterial PTE.

For substrates such as **I**, there is little need to protonate the leaving group phenol as the P−O bond of the substrate is cleaved, because the pK_a of *p*-nitrophenol is below the pH of the assay. However, in other members of the amidohydrolase superfamily, the leaving group must be protonated during the course of the reaction. The best characterized example is that of dihydroorotase (DHO), where the amide nitrogen of dihydroorotate must be protonated (*26*, *27*). The only residue within the active site of DHO that can accomplish this task is Asp250. This residue is homologous to Asp301 in PTE and is ligated to the α-metal ion in both enzymes. In DHO, Asp250 abstracts the proton from the bridging hydroxide and subsequently transfers the proton to the amide nitrogen. In PTE, Asp301 is also hydrogen-bonded to His254. The role of this hydrogen-bonded network may be to transfer the proton from the bridging hydroxide away from the active site because it is not required for the hydrolysis of activated organophosphate triesters such as **I**. If this hypothesis is correct, then the mutation of His254 to one that is incapable of proton transfer away from the active site might enable Asp301 to shuttle the proton from the bridging hydroxide directly to the leaving group phenol. When His254 is mutated to alanine and asparagine, the kinetic parameters for the hydrolysis of **I** *diminish* by 1−2 orders of magnitude. In contrast, the kinetic constants for the slow substrate **II** *increase* by 2−33-fold. These results are consistent with a mechanism whereby His254 functions to abstract a proton from Asp301 during the hydrolysis of the fast substrates such as **I**. Additional support for this conjecture is provided by the kinetic properties of the two mutants at residue Asp233. With either D233N or D233A, there is a decrease in the kinetic constants for the hydrolysis of the fast substrate **I** but an increase in the magnitude of the rate constants for the slow substrate **II**. These results are consistent with a proton relay from Asp301 to His254 to Asp233.

Proton-Transfer Steps. D_2O was utilized to probe for the kinetic significance of proton-transfer steps during substrate turnover. With the slow substrate **II**, the effects of D_2O are small for all of the metal-substituted variants tested. This observation suggests that any proton transfers are largely uncoupled from P−O bond cleavage. With the faster substrate **I**, there is no measurable effect on k_{cat}/K_m but a larger effect that averages to ∼2.1 for k_{cat}. For **I** hydrolysis, k_{cat} is limited by an aggregate of steps that follow P−O bond cleavage. With PTE, this process likely involves the regeneration of the bridging hydroxide from water within the binuclear metal center. The deuterium solvent isotope effects are essentially unchanged for the D233, H254, and D301 mutants, relative to the wild-type enzyme.

Mechanism of Action. The kinetic and structural data obtained for the bacterial PTE have been assembled to formulate a chemical mechanism for the binding and hydrolysis of the substrates. In the free enzyme, a bound hydroxide bridges the two divalent cations. The pH-rate profiles obtained with fast and slow substrates indicate that the catalytic activity is lost at a low pH because of the protonation of the bridging hydroxide. The pK_a of this ionization is primarily due to the identity of the divalent cation that occupies the α site. Substrate binds to the active

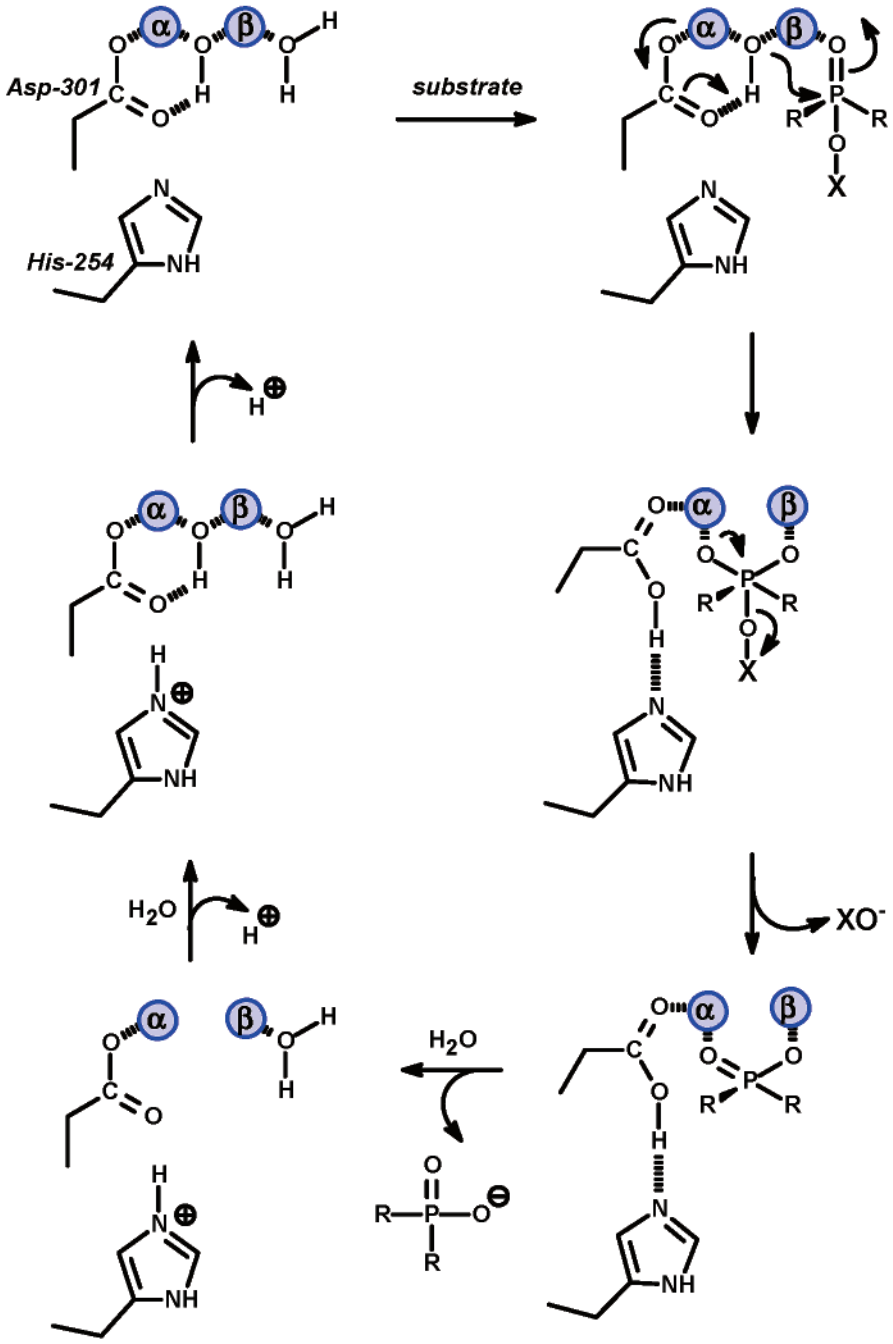

FIGURE 6: Model for the chemical-reaction mechanism of the bacterial PTE.

site in an orientation that polarizes the P−O bond of phosphate esters through ligation of the phosphoryl oxygen with the divalent cation at the β site. Structural support for this proposal is obtained from the structure of diisopropyl methylphosphonate (DIMP) at the active site (*23*) and the differential rate enhancement for the Zn/Cd hybrid PTE for the hydrolysis of thiophosphate esters. A portion of the active site structure with bound DIMP is presented in Figure 5. In this figure, we have taken the liberty of proposing the relative positions of the hydrogen and unligated lone pair for the bound hydroxide. In this two-dimensional representation, the hydroxide is above the vector that connects the two divalent cations. The hydrogen from the bridging hydroxide is orientated toward the carboxylate oxygen of the primary metal ligand Asp301, whereas the lone pair is positioned in the opposite direction toward the phosphorus center of the bound substrate analogue. The side chains of Asp301 and His254 are uniquely positioned to shuttle the protons away from the active site.

The chemical mechanism for the hydrolysis of organophosphate triesters by PTE is presented in Figure 6. Upon binding of the substrate to the active site, there is a nucleophilic attack on the phosphorus center and proton transfer to Asp301. The complexation of the phosphoryl oxygen of the substrate to the β metal may weaken the binding of the hydroxide to the β-metal ion as previously observed in the structure of dihydroorotate bound to the active site of dihydroorotase (*26*). The P−O bond is broken and an enzyme−product complex forms as a phosphate anion that bridges the two divalent cations. The proton is shuttled away from the active site with the assistance of His254 and Asp233. The product is released, and the active-site hydrox-

ide is regenerated, although the details for how this happens have not been specifically addressed in this investigation. For fast substrates such as **I** ($k_{cat} = \sim 10^4\ s^{-1}$), the regeneration of the resting state of the enzyme is largely rate-limiting and dependent on the proton-transfer steps. Further support for this mechanism is being sought through the acquisition of ultrahigh-resolution crystal structures of PTE with substrate and inhibitor complexes.

ACKNOWLEDGMENT

We thank Dr. Lisa Perez for her assistance with the computer graphic representations of the active site of PTE.

REFERENCES

1. Dumas, D. P., Caldwell, S. R., Wild, J. R., and Raushel, F. M. (1989) Purification and properties of the phosphotriesterase from *Pseudomonas diminuta*, *J. Biol. Chem. 264*, 19659−19665.
2. McDaniel, C. S., Harper, L. L., and Wild, J. R. (1988) Cloning and sequencing of a plasmid-borne gene (opd) encoding a phosphotriesterase, *J. Bacteriol. 170*, 2306−2311.
3. Kuo, J. M., and Raushel, F. M. (1994) Identification of the histidine ligands to the binuclear metal center of phosphotriesterase by site-directed mutagenesis, *Biochemistry 33*, 4265−4272.
4. Omburo, G. A., Kuo, J. M., Mullins, L. S., and Raushel, F. M. (1992) Characterization of the zinc binding site of bacterial phosphotriesterase, *J. Biol. Chem. 267*, 13278−13283.
5. Yang, H., Carr, P. D., McLoughlin, S. Y., Liu, J. W., Horne, I., Qiu, X., Jeffries, C. M., Russell, R. J., Oakeshott, J. G., and Ollis, D. L. (2003) Evolution of an organophosphate-degrading enzyme: a comparison of natural and directed evolution, *Protein Eng. 16*, 135−145.
6. Dumas, D. P., Durst, H. D., Landis, W. G., Raushel, F. M., and Wild, J. R. (1990) Inactivation of organophosphorus nerve agents by the phosphotriesterase from *Pseudomonas diminuta*, *Arch. Biochem. Biophys. 277*, 155−159.
7. Koepke, J., Scharff, E. I., Lucke, C., Ruterjans, H., and Fritzsch, G. (2002) Atomic resolution crystal structure of squid ganglion DFPase, *Acta Crystallogr., Sect. D 58*, 1757−1759.
8. Lewis, V. E., Donarski, W. J., Wild, J. R., and Raushel, F. M. (1988) Mechanism and stereochemical course at phosphorus of the reaction catalyzed by a bacterial phosphotriesterase, *Biochemistry 27*, 1591−1597.
9. Benning, M. M., Kuo, J. M., Raushel, F. M., and Holden, H. M. (1994) Three-dimensional structure of phosphotriesterase: an enzyme capable of detoxifying organophosphate nerve agents, *Biochemistry 33*, 15001−15007.
10. Holm, L., and Sander, C. (1997) An evolutionary treasure: unification of a broad set of amidohydrolases related to urease, *Proteins 28*, 72−82.
11. Shim, H., and Raushel, F. M. (2000) Self-assembly of the binuclear metal center of phosphotriesterase, *Biochemistry 39*, 7357−7364.
12. Koca, J., Zhan, C. G., Rittenhouse, R. C., and Ornstein, R. L. (2001) Mobility of the active site bound paraoxon and sarin in zinc-phosphotriesterase by molecular dynamics simulation and quantum chemical calculation, *J. Am. Chem. Soc. 123*, 817−826.
13. Donarski, W. J., Dumas, D. P., Heitmeyer, D. P., Lewis, V. E., and Raushel, F. M. (1989) Structure−activity relationships in the hydrolysis of substrates by the phosphotriesterase from *Pseudomonas diminuta*, *Biochemistry 28*, 4650−4655.
14. Caldwell, S. R., Newcomb, J. R., Schlecht, K. A., and Raushel, F. M. (1991) Limits of diffusion in the hydrolysis of substrates by the phosphotriesterase from *Pseudomonas diminuta*, *Biochemistry 30*, 7438−7444.
15. Ho, S. N., Hunt, H. D., Horton, R. M., Pullen, J. K., and Pease, L. R. (1989) Site-directed mutagenesis by overlap extension using the polymerase chain reaction, *Gene 77*, 51−59.
16. Kuo, J. M., Chae, M. Y., and Raushel, F. M. (1997) Perturbations to the active site of phosphotriesterase, *Biochemistry 36*, 1982−1988.
17. Schowen, K. B., and Schowen, R. L. (1982) Solvent isotope effects of enzyme systems, *Methods Enzymol. 87*, 551−606.
18. Hong, S. B., and Raushel, F. M. (1996) Metal-substrate interactions facilitate the catalytic activity of the bacterial phosphotriesterase, *Biochemistry 35*, 10904−10912.
19. Barnum, D. W. (1983) Hydrolysis of cations. Formation constants and standard free energies of formation of hydroxy complexes, *Inorg. Chem. 22*, 2297−2305.
20. He, C., and Lippard, S. J. (2000) Modeling carboxylate-bridged dinuclear active site in metalloenzymes using a novel naphthyridine-based dinucleating ligand, *J. Am. Chem. Soc. 122*, 184−185.
21. Kaminshaia, N. V., He, C., and Lippard, S. J. (2000) Reactivity of μ-hydroxodizinc (II) center in enzymatic catalysis through model studies, *Inorg. Chem. 39*, 3365−3373.
22. Benning, M. M., Shim, H., Raushel, F. M., and Holden, H. M. (2001) High-resolution X-ray structures of different metal-substituted forms of phosphotriesterase from *Pseudomonas diminuta*, *Biochemistry 40*, 2712−2722.
23. Benning, M. M., Hong, S. B., Raushel, F. M., and Holden, H. M. (2000) The binding of substrate analogues to phosphotriesterase, *J. Biol. Chem. 275*, 30556−30560.
24. Vanhooke, J. L., Benning M. M., Raushel, F. M., and Holden, H. M. (1996) Three-dimensional structure of the zinc-containing phosphotriesterase with the bound substrate analogue diethyl 4-methylbenzylphosphonate, *Biochemistry 35*, 6020−6025.
25. Omburo, G. A., Mullins, L. S., and Raushel, F. M. (1993) Structural characterization of the divalent cation sites of bacterial phosphotriesterase by ^{113}Cd NMR spectroscopy, *Biochemistry 32*, 9148−9155.
26. Thoden, J. B., Phillips, G. N., Jr., Neal, T. M., Raushel, F. M., and Holden, H. M. (2001) Molecular structure of dihydroorotase: a paradigm for catalysis through the use of a binuclear metal center, *Biochemistry 40*, 6989−6997.
27. Christopherson, R. I., and Jones, M. E. (1979) Interconversion of carbamoyl-L-aspartate and L-dihydroorotate by dihydroorotase from mouse Ehrlich ascites carcinoma, *J. Biol. Chem. 254*, 12506−12512.

BI0497805